Published in final edited form as:
Nanotechnology. 2011 July 8; 22(27): 275606. doi:10.1088/0957-4484/22/27/275606.

Fluorescent magnetic hybrid nanoprobe for multimodal bioimaging

Dmitry Koktysh[a,b], **Vanessa Bright**[c], and **Wellington Pham**[c,d,e]

[a]Department of Chemistry, Vanderbilt University, Station B 351822, Nashville, TN 37235, USA

[b]Vanderbilt Institute of Nanoscale Science and Engineering, Vanderbilt University, Station B 350106, Nashville, TN 37235, USA

[c]Institute of Imaging Science, Vanderbilt University, 1161 21st Avenue South AA. 1105 MCN, Nashville, TN 37232, USA

[d]Department of Radiology and Radiological Sciences, Vanderbilt University, 1211 Medical Center Drive, Nashville, TN 37232, USA

[e]Department of Biomedical Engineering, Vanderbilt University, Station B 35163, Nashville, TN 37235, USA

Abstract

A fluorescent magnetic hybrid imaging nanoprobe (HINP) was fabricated by conjugation of superparamagnetic Fe_3O_4 nanoparticles and visible light-emitting (~600 nm) fluorescent CdTe/CdS quantum dots (QDs). The assembly strategy used the covalent linking of the oxidized dextran shell of magnetic particles to the glutathione ligands of QDs. Synthesized HINP formed stable water-soluble colloidal dispersions. The structure and properties of the particles were characterized by transmission electron and atomic force microscopy, energy dispersive X-ray analysis and inductively coupled plasma optical emission spectroscopy, dynamic light scattering analysis, optical absorption and photoluminescence spectroscopy, and fluorescent imaging. The luminescence imaging region of the nanoprobe was extended to the near-infrared (NIR) (~800 nm) by conjugation of superparamagnetic nanoparticles with synthesized CdHgTe/CdS QDs. Cadmium, mercury based QDs in HINP can be easily replaced by novel water soluble glutathione stabilized $AgInS_2$/ZnS QDs to present a new class of cadmium-free multimodal imaging agents. Observed NIR photoluminescence of fluorescent magnetic nanocomposites supports their use for bioimaging. The developed HINP provides dual-imaging channels for simultaneous optical and magnetic resonance imaging.

1. Introduction

The development of the multimodal imaging agent described in this work involves nanoprobes that combine both magnetic and optical properties. Usually these imaging modalities serve in a complementary fashion to each other. One highly desirable example of a multimodal agent is the magnetic resonance (MR) imaging probe with fluorescent capability, this offering great potential for biological imaging [1]. Optical and MR imaging

Correspondence to: Dmitry Koktysh; Wellington Pham.

dmitry.koktysh@vanderbilt.edu, wellington.pham@vanderbilt.edu.

techniques have enabled simultaneous labeling and tracking of cells *in vitro* and in *vivo*, albeit using separate probes for each modality. MR imaging provides excellent spatial resolution on the order of tens of a microns per voxel for animal and human cells and tissue [2], while fluorescent optical imaging provides optical resolution of function and structures on mouse model and cell lines [3]. The principal objective of this work has been to develop a multimodal probe that provides all the benefits of each imaging modality in a single probe [4].

Current examples of multimodal imaging agents include nanocomposites containing magnetic particles and quantum dots (QDs) [5, 6]. Superparamagnetic iron oxide (SPIO) nanoparticles (NPs) are widely utilized as FDA-approved contrast agents for MRI clinical imaging [7]. QDs are increasingly used as fluorophores for *in vitro* and *in vivo* fluorescent imaging due to their high photostability, broad excitation and tuned narrow emission spectra [8]. Numerous strategies have been developed to combine magnetic and fluorescent nanoparticles into one imaging nanoprobe. These include incorporation or encapsulation of both types of particles in silica or polystyrene beads, coating the SPIO particles with QDs or vice versa [5, 6, 9]. One of the major requirements of multimodal probes is the retention of their dual-imaging performance. The preservation of imaging functionalities of the fluorescent magnetic nanocomposites has to be achieved by careful design and an extremely accurate synthesis methodology [5]. For imaging applications, chemical instability and aggregation of the fabricated imaging probes should also be prevented. Depending on the goals of the bioimaging study, different properties (size, composition, optical properties) of the multimodal agents may also be required [6].

In this work we demonstrate a simple technique for the fabrication of hybrid imaging nanoprobes (HINP) based on water soluble SPIO NPs and QDs. This synthetic technique uses covalent binding of glutathione coated visible CdTe/CdS or near-infrared (NIR) light emitting CdHgTe/CdS QDs to SPIO particles functionalized by dextran. To take advantage of this universal approach toward fabrication of hybrid particles, cadmium-free glutathione stabilized $AgInS_2$/ZnS QDs were used as well. The resulting imaging probe possesses the attributes required for both MR and fluorescent imaging in a single system.

2. Experimental

2.1. Materials

Ferric chloride hexahydrate (99%), ferrous chloride tetrahydrate (99%), zinc chloride (98%), silver nitrate (99.8%) oleylamine (OLA) (70%) and dextran (M.w. 20000) were purchased from Sigma-Aldrich. Cadmium chloride hemipentahydrate (99.9%), mercury acetate (99%), glutathione (GSH) (98%), tetramethylammonium hydroxide (TMAH) (25% solution in methanol) were purchased from Acros Organics and sodium borohydride (98%), tellurium (99.999%), thioacetamide (TAA) (98%), sodium diethyldithiocarbamate (98%), indium acetate (99%) were purchased from Alfa Aesar. Organic solvents used were of analytical reagent grades.

2.2 Synthesis of QDs and SPIO nanoparticles

CdTe/CdS QDs were prepared by a modified procedure published elsewhere [10]. Briefly, 40 mg of $NaBH_4$ were dissolved in 2 mL of H_2O contained in a small vial with a septum and cooled with ice. 64 mg of Te powder were added to a solution of $NaBH_4$ and stirred until completely dissolved under constant cooling conditions and slow Ar flow. The resulting clear solution of NaHTe was transferred into 50 mL of degassed water. At the same time, 46 mg of cadmium chloride and 122 mg of GSH were dissolved in 50 mL of H_2O. The pH of the resulting Cd-GSH complex was adjusted to 10 by adding 1M NaOH solution dropwise. All solutions were purged for about 30 min with Ar before further use.

CdTe QDs were prepared by injection of 5 mL of NaHTe solution into a Cd-GSH solution, which was then heated at 100 °C for 1 hour. The QDs luminescence can be tuned by adjusting the particle size through variation of the heating time. Core-shell CdTe/CdS QDs were prepared by overcoating the synthesized core QDs with CdS. Briefly, 3.8 mg of TAA were added to synthesized CdTe QDs at 100 °C and the mixture was refluxed for 40 min. Excess precursors were washed from the CdTe/CdS QDs by flocculating the solution with isopropanol and isolating the QDs by centrifugation. The desired visible light emitting CdTe/CdS QDs were redissolved in 10 mL of H_2O.

The NIR emitting CdHgTe/CdS QDs were synthesized in the same manner as CdTe/CdS QDs except 3 mg of mercury acetate were added into the Cd-GSH mixture before further processing.

$AgInS_2$/ZnS QD were synthesized according to [11, 12]. $AgInS_2$/ZnS QDs were transferred into the aqueous phase by a ligand exchange using a procedure [13] with the following modifications. For this, 20 mg of glutathione was dispersed in 1 mL of methanol. The pH of the GSH solution was adjusted to 12 by dropwise addition of TMAH. At this point the methanol solution of GSH turned completely transparent. The prepared GSH methanolic solution was added dropwise into a QDs chloroform solution under vigorous stirring and left while still stirred for 20 hours. Then, 1 mL of water was added into a mixture and the solution was vigorously shaking. Complete transfer of the QDs to the aqueous phase was observed. The mixture was separated into an organic and aqueous phase by centrifuging at 4500 rpm for 10 min. Extracted QDs were washed with acetone several times and dissolved in water forming a clear solution.

The SPIO NPs were synthesized based on a previously reported protocol with some modifications [14, 15]. Specifically, the dextran (DX) (15 g) was mixed with ferric chloride (0.2 M) and ferrous chloride (0.1 M) in 5 mL of H_2O. The pH of the solution was raised to 10 by dropwise addition of 30 % solution of ammonium hydroxide. The temperature of the reaction mixture was raised from room temperature to 75 °C and the solution was heated at this temperature for 2 h. The resulting SPIO-DX NPs were purified from the excess of dextran and other starting materials using microcentrifugation in physiological pH eluant (20 mM sodium citrate and 0.15 M NaCl).

2.3. Conjugation of QDs and SPIO nanoparticles

The dextran shell of SPIO-DX NPs was partially oxidized according to a reported procedure [16, 17]. Briefly, to SPIO NPs (5 mg in 0.5 mL of 0.2 M acetate buffer, pH 6) was added $NaIO_4$ (5 mg in 0.5 mL of 0.2 M acetate buffer, pH 6). The mixture was stirred for 1 hour at 22 °C in the dark. The resulting SPIO-DX_{ox} NPs were dialyzed extensively by using Slide-A-Lyser cassette (20,000 MWCO) in 0.15 M NaCl. 1 mg of washed NPs was concentrated using a Microcon Centrifugal Unit (Ultracel YM-100, MWCO=100,000) at 10,000 rpm for 12 min and redispersed in 0.4 mL of borate buffer (0.2 M, pH 8). To this solution 0.1 mL of QDs were added and the mixture was stirred for 20 hours at 22 °C. Then, 0.025 mL freshly prepared 1% $NaBH_4$ solution were added and the solution was stirred for 15 min. The final product was separated from the excess of unconjugated QDs using the Microcon Centrifugal Unit (Ultracel YM-100, MWCO=100,000) at 10,000 rpm for 12 minutes. The washing procedure was repeated 6 times.

2.4. Characterization

HRTEM images were obtained using a Philips CM20 TEM operating at 200 kV. The samples for TEM investigation were prepared by adding drops of the solution of washed NPs onto carbon coated copper grids (Ted Pella, 400 mesh) and wiping off the excess liquid.

Energy dispersive X-ray analysis (EDAX) analysis was conducted using the same TEM microscope and samples.

Atomic force microscopy (AFM) images were obtained using a Nanoscope IIIa (Veeco) in taping mode using silicon cantilevers. The samples for AFM imaging were prepared by assembling the NPs onto a cleaned silicon wafer with an underlying polyelectrolyte layer following the adapted procedure noted elsewhere [18, 19].

The hydrodynamic diameter (HD) and zeta potential of the particles was determined using a Zetasizer Nano ZS (Malvern Instruments, UK). Zetasizer incorporates non-invasive backscatter (NIBS) optics and a 633nm laser. The particle size was measured at 25 °C.

The particle's composition was determined using an inductively coupled plasma optical emission spectrometer (ICP-OES, Perkin-Elmer Optima 7000). To obtain the desired concentration of elements for analysis, a 50 μL of particle's solution was dissolved in 1 mL of aqua regia and diluted by 5 % nitric acid solution to 40 mL of analyzed solution.

Absorption spectra of aqueous solutions of NPs were measured at room temperature with a Cary 5000 UV-vis-NIR spectrometer (Varian). The photoluminescence spectra of NPs were recorded with a Fluorolog-3 FL3-111 (Jobin Yvon/Horiba).

FTIR spectroscopy was conducted using a Bruker Tensor 27 equipped with a Seagull ATR accessory. A Ge-ATR hemispherical crystal was used to collect ATR spectra.

The CRI Maestro system (CRi) was used for fluorescence imaging. The object was put into a microcentrifuge tube. For HINP containing visible or NIR QDs the excitation filter was set at 480 nm and 690 nm, respectively. The fluorecence spectra were scanned from 500-700 nm for visible HINP and 730-950 nm for NIR HINP.

ImageJ (NIH, Wayne Rasband) was used for processing and analysis of the captured images.

2.5. Distribution of the HINP probe in an vivo mouse model using nebulization

The optical-magneto aerosol was generated from the NIR HINP using an Aeroneb Lab Control Module system. To convey the particle aerosol to the nose of mice (n =3), the system was attached to a custom designed spray nozzle and carrier oxygen inlet. The velocity of the spray is on the order of 3-5 inches per second. Using this controlled flow, the aerosol spray was guided to the nose of the mouse by an air sheet and propelled toward the animal in uniform aerosol particles.

Twenty four hours after nebulization, mice were sacrificed and the mediastinal lymph nodes were dissected and imaged using the Maestro CRi optical imaging system (Woburn, MA). The excitation filter set was selected at 690 nm which is equivalent to deep red, and the emission filter set was 750-800 nm.

3. Results and Discussion

The schematic presentation of the hybrid imaging probe assembly is shown in figure 1(a). The conjugate consisted of SPIO and QDs counterparts. The actual assembly of magnetic and fluorescent parts was based on covalent linking of the nanoparticle ligands – dextran and glutathione, respectively. For the covalent linking of QDs-GSH and SPIO-DX the dextran backbone needs to be activated. The activation of dextran is typically effected by using cyanobromide [20] but this process possesses potential hazard issues connected to the high toxicity activation molecule together with instability of the formed conjugate [21]. In this work the activation of dextran coated SPIO NPs (figure 1(b)) was achieved by the

simple route of transforming the relatively unreactive hydroxyls of sugar residues into amine-reactive aldehydes by partial oxidation with periodate [22].

Periodate cleaves carbon–carbon bonds that possess adjacent hydroxyls, oxidizing the -OH groups to form highly reactive aldehydes [22]. The presence of aldehydes was checked by a 2,4-dinitrophenylhydrazine (DNPH, Brady's reagent) method [23, 24]. A positive test was signaled by the formation of a yellow precipitate upon addition of dextran aldehyde coated SPIO to a DNPH reagent [23] compared to a negative test in the case of the original dextran coated SPIO NPs. Further, imine bonds formed due to the Schiff base interactions between dextran aldehyde functionalized SPIO NPs and amine groups from added glutathione coated QDs. The imine bonds were finally reduced to permanent secondary amine bonds by sodium borohydride.

FTIR analysis showed the presence of bands: 3306 cm^{-1} (overlapping OH and NH_2 stretching), 2924 cm^{-1} (CH_2 symmetric stretching), 1603 cm^{-1} (NH bending), 1397 cm^{-1} (CN stretching), 1024 cm^{-1} (CO stretching) for HINP nanoparticles consisting of QDs and SPIO nanoparticles (figure S1).

TEM images of SPIO, QDs and HINP nanoparticles are presented in figure 2. CdTeCdS QDs stabilized by glutathione used for conjugation had a size of 2.5 nm compare to the size of SPIO particles of 5.8 nm. The average TEM size of the conjugated particles was estimated to be ~7.8 nm with minimum aggregation.

In addition, the structural compostion of formed luminescent magnetic nanoparticles can be verified by EDS or EDAX analysis [25, 26]. EDAX analysis of composite particles showed the presence of major peaks due to Fe, Cd in their structure(figure 2(d)). Fe peaks were characteristic of SPIO NPs. At the same time the Cd peak indicated the presence of CdTe/CdS QDs further verified by EDAX analysis of CdTe/CdS QDs (figure 2(d).Inset).

ICP-OES elemental analysis showed 87% of Fe and 13% of Cd for analysed composite nanoparticles which is in agreement with the EDAX data showing 85.1% of Fe and 14.9% of Cd.

Dynamic light scattering analysis (DLS) analysis verified the conjugation of QDs to activated SPIO NPs. As evidenced from figure 3(a), periodate oxidation of dextran coated SPIO NPs did not lead to noticeable particle size increase compared to the HD enlargement of composite particles from 29 nm of SPIO NPs to 44 nm SPIO NPs conjugated to QDs (table 1). Discrepancies between the particle sizes estimated by TEM and DLS analysis can be explained by the presence of hydration shell at the particle surface. The mixing of non-activated SPIO NPs and QDs did not lead to particle size enlargement compared to the composite particles. This provides additional evidence that the proposed HINP synthetic procedure (figure 3) was effective. The DLS measurements also indicated that the majority of SPIO particles were coupled to semiconductor QDs as evidenced by a monomodal size distribution. No agglomeration was observed as further verified by in-situ DLS analysis.

The AFM images of SPIO-DX and HINP particles are presented in figure S2. Nearly round particles with minimal aggregation were formed during the conjugation of QDs to SPIO NPs (figure S2(b)). The AFM imaging clearly indicates that the conjugation of QDs to SPIO NPs increases the size of the final nanocomposite while maintaining the relatively narrow size distribution.

The measured Zeta potential of the conjugated particles was slightly more negative (-15 mV) than that of just SPIO-DX NPs (-11 mV). Indeed, covalent coupling led to the

formation of SPIO conjugates with glutathione coated QDs which have a stronger negative charge due to the available deprotonated carboxylic groups.

Absorption and photoluminescence spectra of CdTe/CdS QDs and HINP NPs in aqueous solutions are shown in figure 4. A PL peak shift from 598 to 607 nm was observed for the formed nanocomposite. The linking of QDs to SPIO NPs using a long molecular linker such as dextran-glutathione helps to avoid strong quenching by the paramagnetic core [5]. The luminescent magnetic nanocomposites can be easily detected with a regular UV lamp (figure 5(a)).

The composite nanoparticles can be separated from solution by magnetic decantation using a magnetic separation unit (LifeSep 15SX, Dexter Magnetic Technologies) (figure 5(b,c)) revealing the magnetic nature of the formed nanocomposites. At the same time NPs collected by magnetic decantation showed photoluminescence as additional evidence of the successful conjugation of SPIO and QDs.

Fluorescent imaging was additionally conducted using a Maestro imaging system (figure 6). A uniform visible fluorescence was observed. The sample was checked for seven days: the probe retained 90% of its original intensity and there was no shift in emission wavelength.

For optical bioimaging NIR luminescence offers key advantages over visible emission because light absorption and scattering from biological tissues is minimized in the NIR region [27-29]. For these reasons, NIR emitting CdHgTe/CdS QDs were synthesized. The emission wavelength of NIR QDs was tuned by careful size manipulation to 800 nm (figure S3(a)). The HINP fabricated from these QDs retained the NIR photoluminescence spectral performance (figure S3(b)). Moreover, the bright NIR photoluminescence was observed as well in phantom imaging demonstrating the necessary requirements for successful practical implementation of HINP for in-vivo bioimaging (figure S4).

As our dual imaging agent was constructed from dextran coated SPIO NPs and glutathione stabilized QDs the toxicity of the resulting nanocomposites should potentially be less than QDs stabilized by other types of ligands, i.e. mercaptopropionic acid since dextran is biocompatible and glutathione is present in large amounts in cellular environments as an antioxidant [30]. The successful use of glutathione coated QDs for fluorescent cell labeling [31] and SPIO NPs for dendritic cell tracking [32] allows one to infer that the use of the nanocomposite system described in this work may well constitute a pending further advance in multimodal bioimaging. However, there are some safety concerns associated to the use of cadmium or mercury containing QD for in vivo optical imaging. Particularly, in the area of cell tracking, highly toxic QDs may hinder the work given cell death is prominent upon adaptively transferred to the host. In this regard, cadmium-free $AgInS_2$/ZnS QDs were synthesized and successfully transferred to the aqueous phase using glutathione. As the result of the universally applicable conjugation scheme used for cadmium based QDs reported here, a novel cadmium free multimodal imaging agents based on $AgInS_2$/ZnS QDs and SPIO NPs were synthesized and tested. The representative optical properties of this hybrid nanoprobe including absoprtion and photoluminescence spectra are presented in figure S5. The photoluminescence emission of the hybrid probe was tuned to NIR (~800 nm) by adjusting the structure of $AgInS_2$/ZnS QDs used for HINP fabrication. Prominent NIR fluorescence emission of the probe measured by the Maestro imaging system verified the feasibility of using this probe for bioimaging (figure S5.c).

To demonstrate the potential use of the newly developed HINP for imaging the lymph nodes, the particles were delivered into a mouse via inhalation. We didn't observe any register toxicity of the particles in these mice. We could not image the distribution in a whole mouse given the black mouse (C57BL/6) has thick and pigmented skin. However, ex

vivo imaging showed that the particles homed in the lungs (data not shown) and subsequently in the draining lymph nodes (figure S6).

In summary, a luminescent magnetic hybrid imaging probe has been fabricated by the conjugation of dextran coated SPIO NPs activated by periodate oxidation to glutathione stabilized QDs. The resulting nanocomposite particles provide a single system that can be used for simultaneous visible or NIR optical and magnetic resonance imaging.

Supplementary Material

Refer to Web version on PubMed Central for supplementary material.

Acknowledgments

This work was supported by NIH grant R03EB009524, Vanderbilt Institute of Imaging Science and Vanderbilt Institute of Nanoscale Science and Engineering.

References

1. Bakalova R, Zhelev Z, Aoki I, Kanno I. Nat. Photonics. 2007; 1:487.
2. Weissleder R. Nat. Rev. Cancer. 2002; 2:11. [PubMed: 11902581]
3. Michalet X, Pinaud FF, Bentolila LA, Tsay JM, Doose S, Li JJ, Sundaresan G, Wu AM, Gambhir SS, Weiss S. Science. 2005; 307:538. [PubMed: 15681376]
4. Medarova Z, Pham W, Farrar C, Petkova V, Moore A. Nature Medicine. 2007; 13:372.
5. Corr SA, Rakovich YP, Gun'ko YK. Nanoscale Res Lett. 2008; 3:87.
6. Koole R, Mulder WJM, van Schooneveld MM, Strijkers GJ, Meijerink A, Nicolay K. Wiley Interdisciplinary Reviews: Nanomedicine and Nanobiotechnology. 2009; 1:475. [PubMed: 20049812]
7. Modo, MM.; Bulte, JWW. Nanoparticles in Biomedical Imaging. Springer; 2008.
8. Bruchez, MP.; Hotz, CZ. Quantum Dots: Applications in Biology. Methods Mol. Biol.; Totowa, NJ, U.S.: 2007. p. 3742007
9. Quarta A, Di Corato R, Manna L, Ragusa A, Pellegrino T. IEEE Trans. Nanobiosci. 2007; 6:298.
10. Liu YF, Yu JS. J. Colloid Interface Sci. 2009; 333:690. [PubMed: 19215940]
11. Torimoto T, Adachi T, Okazaki K, Sakuraoka M, Shibayama T, Ohtani B, Kudo A, Kuwabata S. J. Am. Chem. Soc. 2007; 129:12388. [PubMed: 17887678]
12. Torimoto T, Ogawa S, Adachi T, Kameyama T, Okazaki KI, Shibayama T, Kudo A, Kuwabata S. Chem. Commun. 2010; 46:2082.
13. Pong BK, Trout BL, Lee JY. Langmuir. 2008; 24:5270. [PubMed: 18412382]
14. Woo K, Hong J. IEEE Trans. Magn. 2005; 41:4137.
15. Mowat P, Franconi F, Chapon C, Lemaire L, Dorat J, Hindre F, Benoit JP, Richomme P, Jeune JJ. NMR Biomed. 2007; 20:21. [PubMed: 16998951]
16. Bogdanov AA, Martin C, Weissleder R, Brady TJ. BBA-Biomembranes. 1994; 1193:212. [PubMed: 7518693]
17. Dutton AH, Tokuyasu KT, Singer SJ. Proc. Natl. Acad. Sci. U. S. A. 1979; 76:3392. [PubMed: 16592679]
18. Grant GG, Koktysh DS, Yun B, Matts RL, Kotov NA. Biomedical Microdevices. 2001; 3:301.
19. Sinani VA, Koktysh DS, Yun BG, Matts RL, Pappas TC, Motamedi M, Thomas SN, Kotov NA. Nano Lett. 2003; 3:1177.
20. Kaneo Y, Fujihara Y, Tanaka T, Ogawa K, Fujita K, Iguchi S. Int. J. Pharm. 1989; 57:263.
21. Mehvar R. J. Controlled Release. 2000; 69:1.
22. Hermanson, GT. Bioconjugate Techniques. Academic Press; San Diego, CA: 1996.
23. Hong RY, Li JH, Qu JM, Chen LL, Li HZ. Chem. Eng. J. 2009; 150:572.

24. Hong X, Guo W, Yuang H, Li J, Liu YM, Ma L, Bai YB, Li TJ. J. Magn. Magn. Mater. 2004; 269:95.
25. Wang DS, He JB, Rosenzweig N, Rosenzweig Z. Nano Lett. 2004; 4:409.
26. Yi DK, Selvan ST, Lee SS, Papaefthymiou GC, Kundaliya D, Ying JY. J. Am. Chem. Soc. 2005; 127:4990. [PubMed: 15810812]
27. Hilderbrand SA, Shao F, Salthouse C, Mahmood U, Weissleder R. Chem. Commun. 2009:4188.
28. Weissleder R. Nat. Biotechnol. 2001; 19:316. [PubMed: 11283581]
29. Weissleder R, Ntziachristos V. Nat. Med. 2003; 9:123. [PubMed: 12514725]
30. Deneke SM, Fanburg BL. Am. J. Physiol. 1989; 257:L163. [PubMed: 2572174]
31. Jin T, Fujii F, Komai Y, Seki J, Seiyama A, Yoshioka Y. Int. J. Mol. Sci. 2008; 9:2044. [PubMed: 19325735]
32. Kobukai S, Baheza R, Cobb JG, Virostko J, Xie JP, Gillman A, Koktysh D, Kerns D, Does M, Gore JC, Pham W. Magn. Reson. Med. 2010; 63:1383. [PubMed: 20432309]

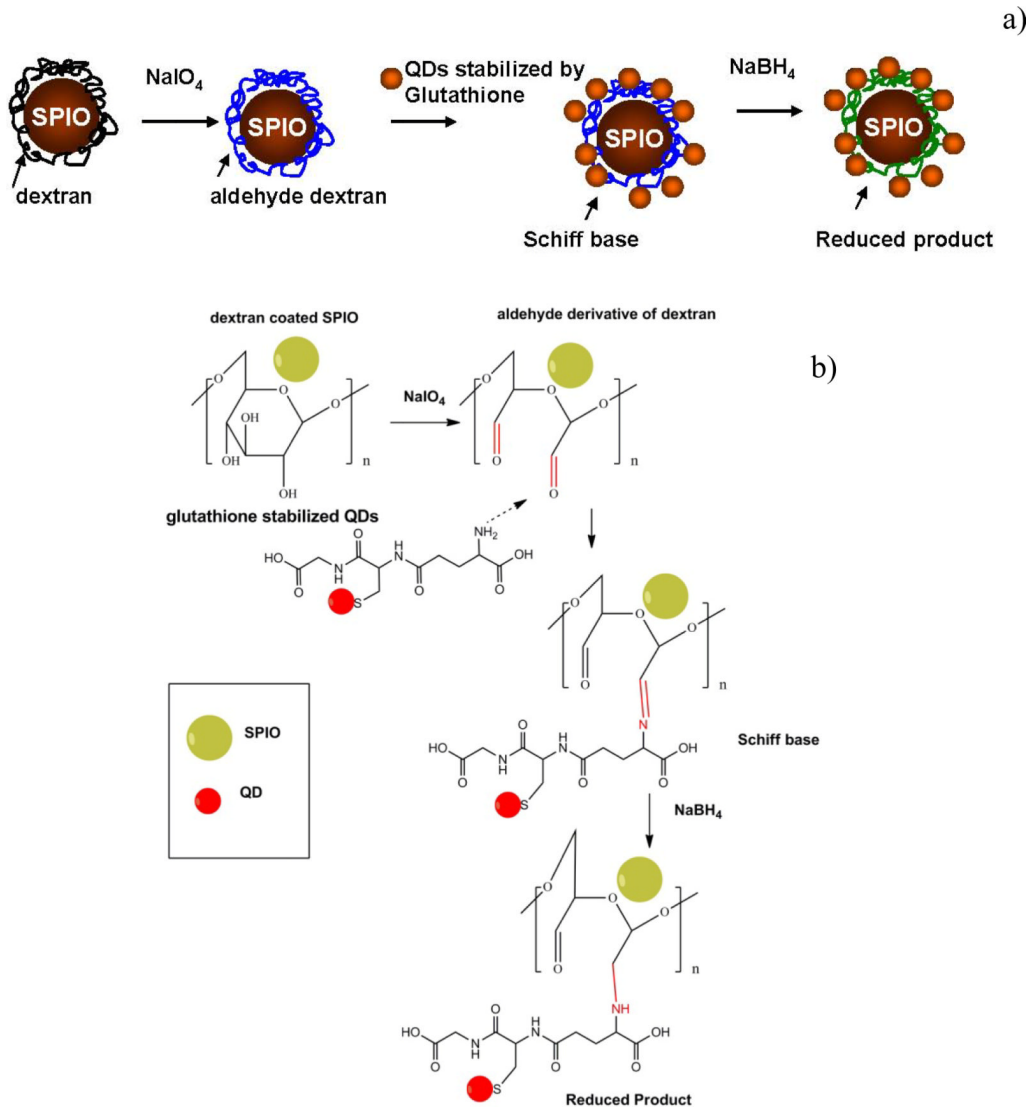

Figure 1.
Schematic diagram illustrating the conjugation of QDs to SPIO nanoparticles (a) and correspondent ligand conjugation mechanism (b).

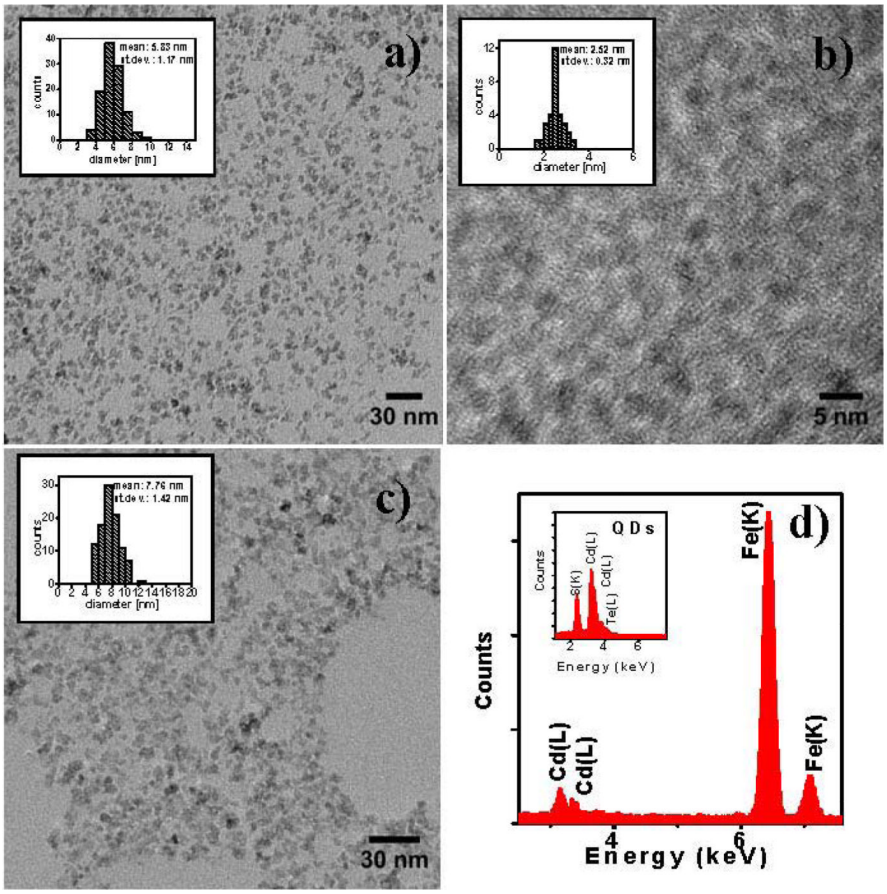

Figure 2.
HRTEM of SPIO (a), QDs (b) and HINP nanoparticles (c) with corresponding EDAX spectra of HINP (d), and QDs (inset).

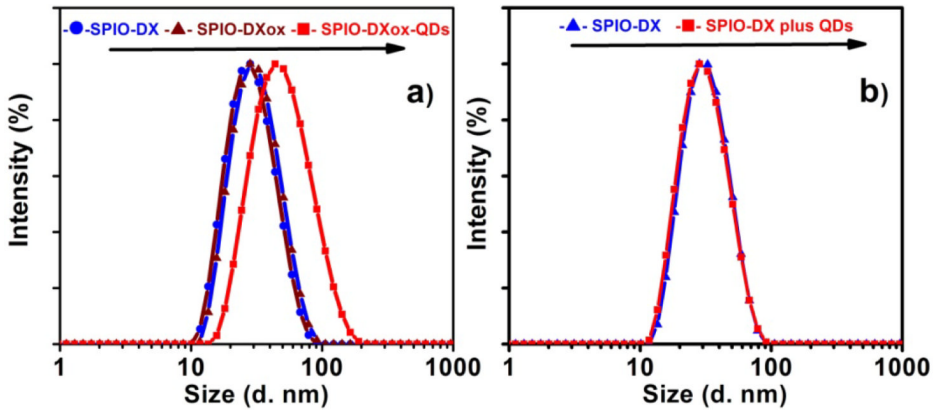

Figure 3.

The hydrodynamic diameter of SPIO-DX, oxidized SPIO-DX_{ox} nanoparticles and QDs conjugated to SPIO-DX_{ox} nanoparticles (a). The hydrodynamic diameter of a mixture of SPIO-DX NPs and QDs is presented for comparison (b).

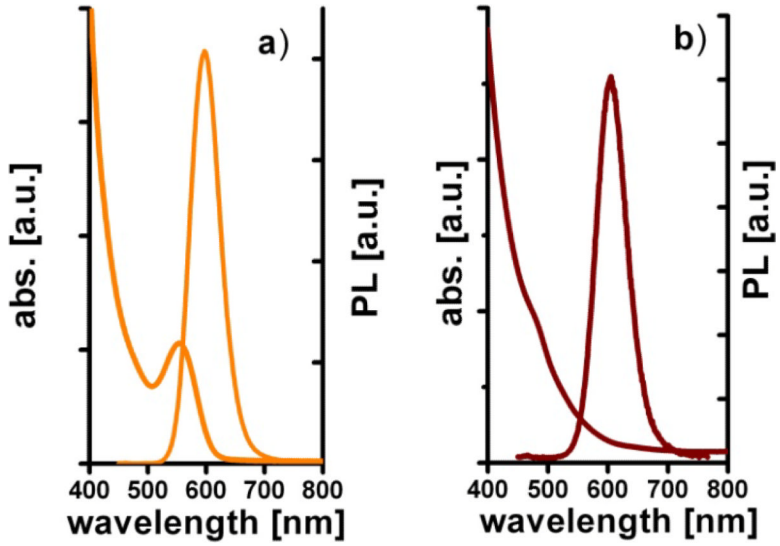

Figure 4.
Absorption and photoluminescence spectra of CdTe/CdS QDs (a) and fabricated HINP (b). The excitation wavelength is 400 nm.

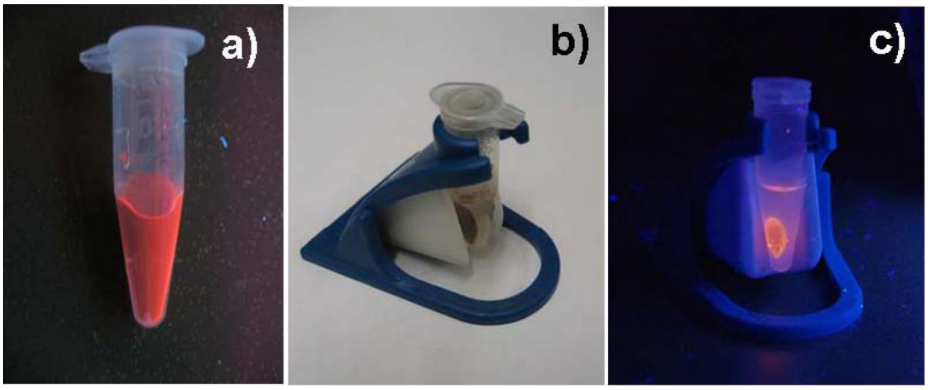

Figure 5.
Photo of photoluminescent HINP under UV-lamp (excitation 365 nm) (a,c) and under ambient illumination (b), in the presence of a magnetic concentrator (b,c).

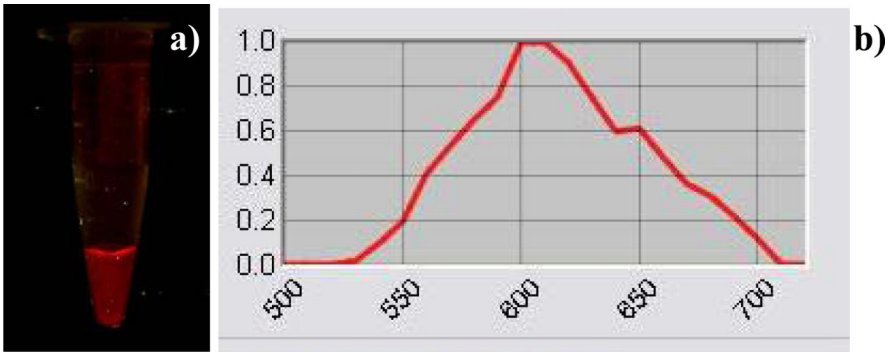

Figure 6.
Fluorescent image of phantom containing visible light emitting HINP (a) and associated fluorescence spectrum (b).

Table 1

Average sizes (Z-average) and polydispersity index (PDI) of SPIO nanoparticles conjugated to QDs.

Sample name	Z-average d.nm	PDI
SPIO-DX	26.8	0.18
SPIO-DXox	28.6	0.14
SPIO-DXox-QDs	43.9	0.215